



Original Article

# Numerical investigation of modal and fatigue performance of a horizontal axis tidal current turbine using fluid–structure interaction

Habib Ullah<sup>a</sup>, Muzamil Hussain<sup>b</sup>, Naseem Abbas<sup>c,\*</sup>, Hassaan Ahmad<sup>a</sup>, Mohammed Amer<sup>d</sup>,  
Muhammad Noman<sup>a</sup>

<sup>a</sup>Faculty of Engineering and Technology, University of Lahore, Lahore 54000, Pakistan

<sup>b</sup>Department of Mechanical Engineering, NFC Institute of Engineering and Technology, Multan 60000, Pakistan

<sup>c</sup>School of Mechanical Engineering, Chung-Ang University, Seoul 06974, Republic of Korea

<sup>d</sup>Department of Mechanical Engineering, National Chiao Tung University, Hsinchu, Taiwan

Received 5 April 2019; received in revised form 15 May 2019; accepted 23 May 2019

Available online 25 May 2019

## Abstract

The tidal power has the potential to play a vital role in a sustainable energy future. The main objective of this paper is to investigate the performance and fatigue life of tidal current turbine (TCT) using fluid structure interaction (FSI) modeling. The performance of TCT was predicted using Ansys CFX. The performance curve, pressure distribution on the blade, and velocity streamline were visualized for eight repetitive analyses at different tip speed ratio. The hydrodynamic load calculated from CFD analysis was transferred to FEA model for investigation of the structural response of TCT. Modal analysis was performed to examine the mode shapes and natural frequencies of TCT. The fatigue analysis were performed and number of cycles and safety factor at different equivalent alternating stresses were investigated. The results of the simulation confirm that the turbine has a maximum value of the coefficient of performance at  $\lambda = 5$ , the turbine operating frequency is not close to its natural frequency, and it is safe under the applied fatigue loads with a high factor of safety.

© 2019 Shanghai Jiaotong University. Published by Elsevier B.V.

This is an open access article under the CC BY-NC-ND license. (<http://creativecommons.org/licenses/by-nc-nd/4.0/>)

**Keywords:** Tidal current turbine; Fluid–structure interaction; Fatigue performance; Computational Fluid Dynamic; Blade element.

## 1. Introduction

Rapid growth in industrialization and population has increased energy requirements [1]. The increasing energy demands and continuously depleting non-renewable energy resources need special attention in order to focus on renewable energy resources [2]. Tidal power has the potential to play a valuable part in worldwide energy requirement [3]. Horizontal axis tidal current turbines (HATCT) and vertical axis tidal current turbines (VATCT) are important emerging technologies to extract hydrokinetic energy from tidal waves in a sustainable manner [4,5]. Their design process and working principle can be adopted from the associated windmills [6]. However several technical aspects are yet to be analyzed in

harnessing hydrokinetic energy from tides due to the harsh and corrosive sea environment [7]. Even that, HATCT experience issues which do not influence wind turbines, for example, cavitation at the tip of the blade [8] and additionally encounter moderately higher bending moments of blade root due to the higher density of water [9]. Moreover, the tidal force can change within a small geographical region [10] due to the seabed and bathymetry conditions, creating a challenge for the design of the cost-effective and long-term reliable structure.

The hydrodynamic tidal forces produce the vibration in a tidal structure which causes the dynamic loads and resonance. Blade vibration with the passage of time leads to the edgewise mode of the blade [11]. The tidal force subjected to tidal current turbine (TCT) changes between two extremes velocities in reverse directions in a short time frame due to the wave action and turbulence within a fluid flow [12]. This fluctuation in tidal force is inimical to the fatigue life of TCT [13] and

\* Corresponding author.

E-mail address: [naseem@cau.ac.kr](mailto:naseem@cau.ac.kr) (N. Abbas).

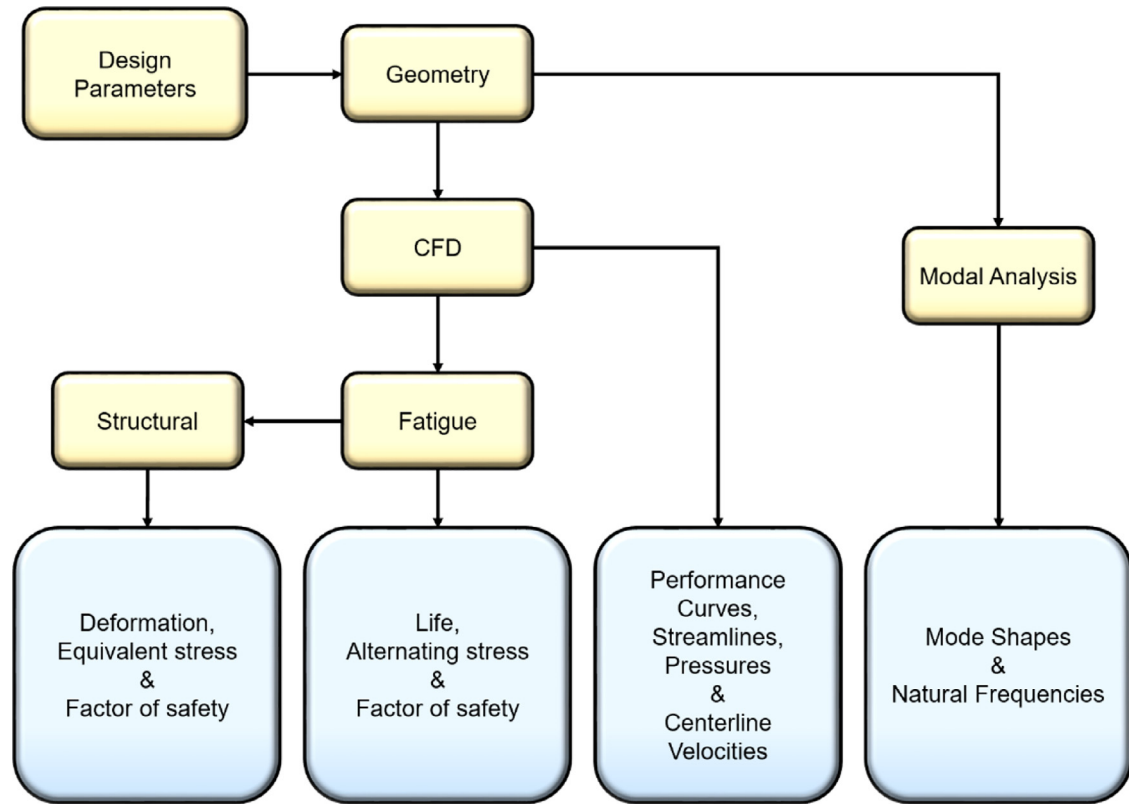


Fig. 1. Computational scheme for modal and fatigue analysis.

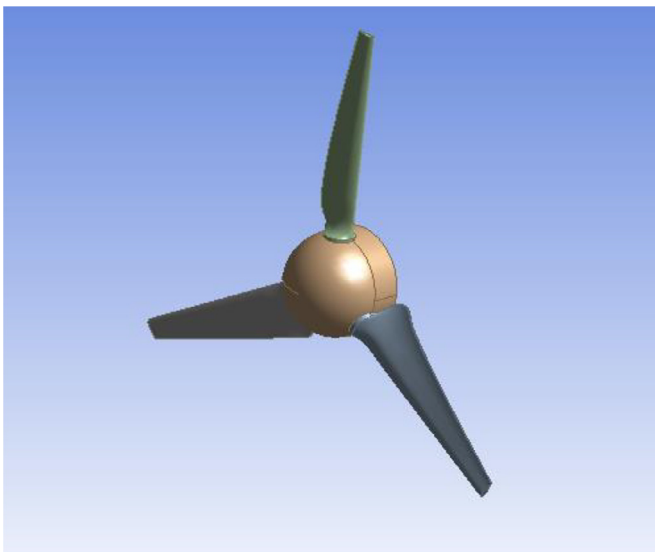


Fig. 2. 3D Geometric model of TCT.

TCT blades are exposed during its lifetime. The fluctuation in fatigue loads depends upon design, specific site area, wave environment and sea bed proximity [14]. Therefore, it is a challenge to analyze the performance of TCT under various type of loadings.

The use of computational methods based on FEM is increasing rapidly to solve the real problems in few years [15]. Computational Fluid Dynamic (CFD) is largely used as a tool

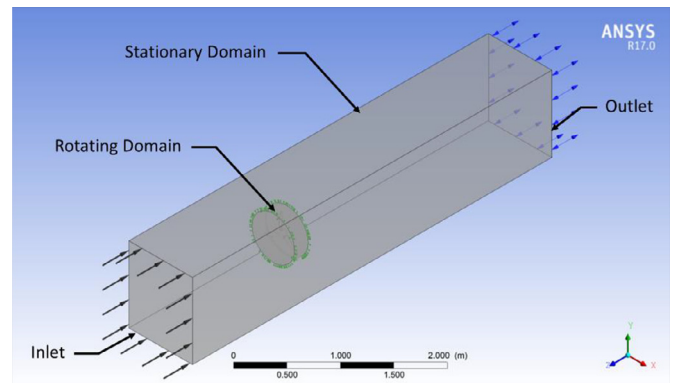


Fig. 3. External and internal flow domains.

for simulating the fluid flows over tidal turbine [16,17]. Blade Element Momentum (BEM), Actuator disc, hydrofoil theories, etc. are largely used as numerical tools for predicting the behavior of tidal current device [18–20]. The use of Large Eddy Simulation (LES) is also increasing for simulating the behavior of the device in the sea environment [21]. For structural analysis, FSI modeling is one of the methods which uses the coupled CFD and FEA methods [22]. Both CFD numerical [22] and experimental methods [23] are suitable for the validation of results. The performance of tidal current turbines has been evaluated experimentally in actual sea conditions by developing actual test model [24,25]. The experimental test method is performed to obtain highly accurate and reliable

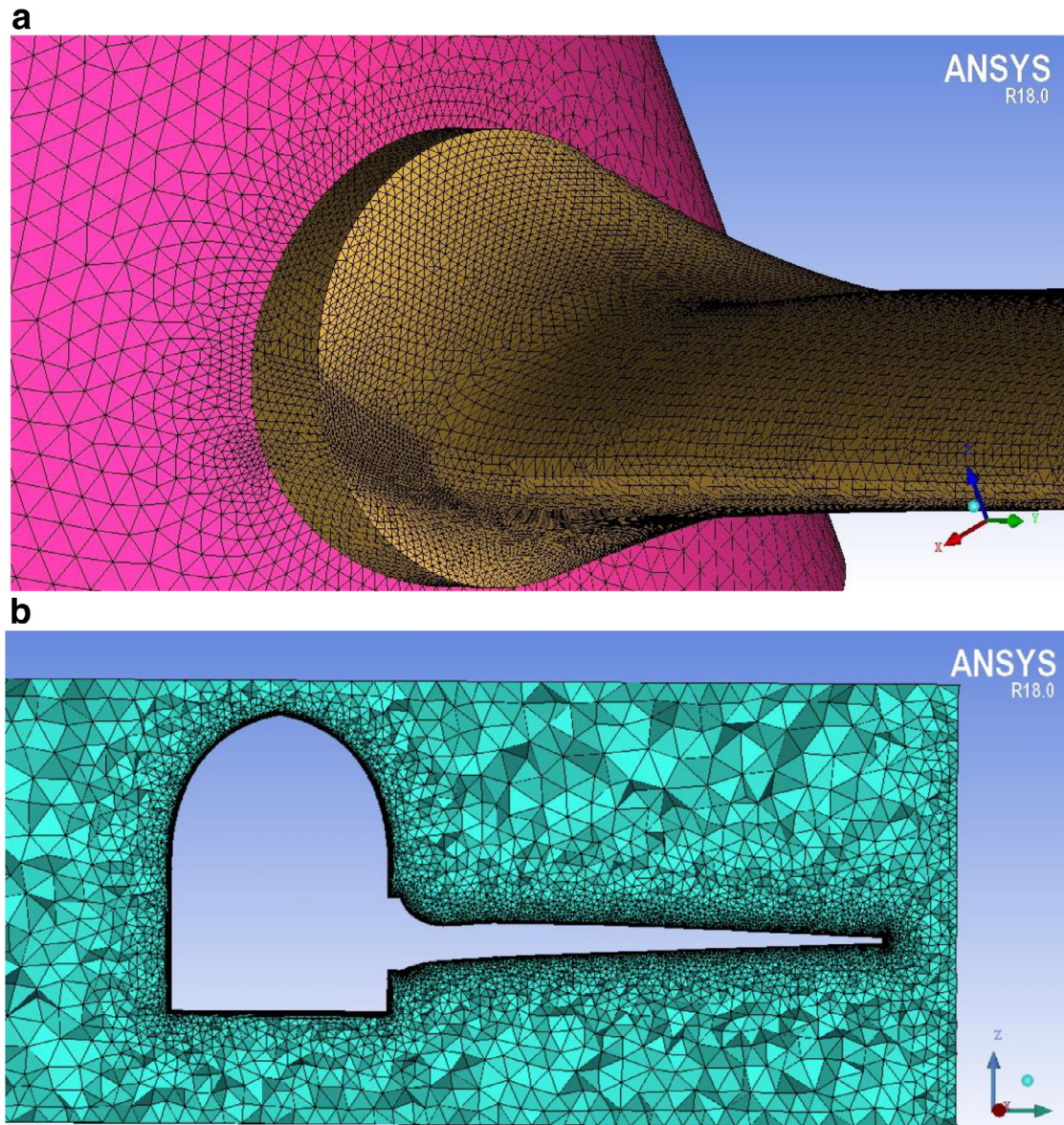


Fig. 4. Grid System (a) hub and blade root (b) section of inner domain.

results but it requires a great deal of time, experience and cost [26]. Therefore, nowadays the numerical method has become more popular for the optimization of tidal turbine performance [27].

Several experimental and computational studies are conducted on TCT. In [10] a setup of HATCT is presented for Pacific Island Countries (PIC). It is investigated that a tremendous and predictable quantity of energy can be generated by utilizing TCT. A 3-bladed computational HATCT model with 10m diameter is also designed in this study. Hydrofoils were considered and designed for various blade position & its hydrodynamic characteristics were analyzed. Fagan et al. [11] presented a design technique for composite blades of TCT. And, they investigated the damage mechanics of fiber failure of carbon-fiber and glass-fiber reinforced composite materials based on the Puck phenomenological

failure criteria. The model is included in a technique for the analysis and design of composite blade of TCT. This technique uses an interactive design procedure with numeral failure criteria to make sure the most favorable structural blade performance. Python programming language is utilized by this technique to facilitate capable variation of model parameters for a variety of design parameters. The blockage effect on tidal turbine performance has been computationally investigated using coupled BEMT-CFD model [26,27]. The Solidity effect on tidal turbine rotor at low flow speed [28] and wake characteristics of HAT turbine [29] have also been numerically studied. The authenticity of computational results using commercially available package FLUENT has been proved after the comparison with experimental results [30]. Kim and co-workers [31,32] utilize FSI method to investigate the effect of deformation on the TCT performance

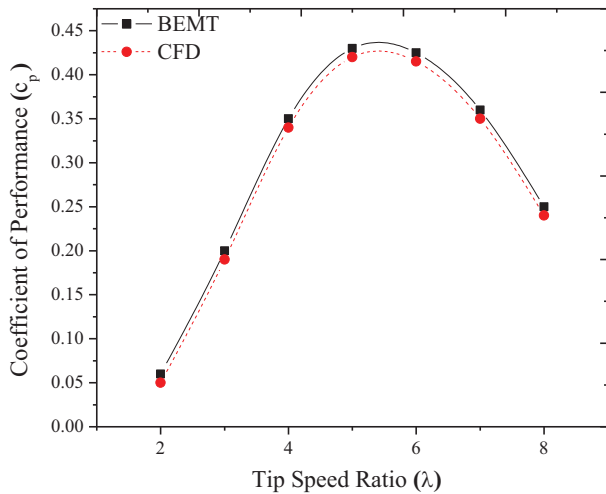


Fig. 5. Performance curve for BEMT and CFD model.

and examined the blade performance after blade deformation. Kim et al. [33] use BEMT CFD simulation to design a 1 MW OCT to predict the performance of the turbine considering cavitation effects. Thus, existing literature indicates that CFD method is a good solution for experimental results.

The computational methodology adopted in previous studies was used to investigate the only limited response of TCT. FSI modeling can evaluate the performance of TCT under any type of loading. Therefore, the FSI modeling was developed to evaluate the modal and fatigue performance of TCT. The CFD analysis was performed in ANSYS CFX to examine the flow phenomenon around the TCT. The pressure distribution in CFD analysis was transferred to FEM model through FSI. The mode shapes and natural frequencies were analyzed performing the modal analysis, whereas fatigue behavior is investigated in static structural based on FSI.

Table 1  
TCT Design Parameters.

Design parameters	Values
Estimated Efficiency ( $\eta$ )	0.9
Power coefficient ( $C_p$ )	0.4
Rated Power ( $P$ )	36.23 W
Water density ( $\rho$ )	1025 kg/m <sup>3</sup>
Number of Blades ( $N$ )	3 EA
Turbine diameter ( $D$ )	0.5 m
Tip Speed Ratio ( $\lambda$ )	5
Rated current velocity ( $U$ )	1 m/s
Angular Speed ( $\omega$ )	191 rpm

## 2. Computational method

The overview of the computational scheme based on FSI modeling is shown in Fig. 1. The detail of each step is explained in the following paragraphs.

### 2.1. Tidal turbine and fluid domain geometry

A three-bladed HATCT based on previous work [24] was modeled for this research work. The geometric model of 0.5 m diameter turbine was designed in Autodesk Inventor Professional 2014 software according to the design parameters of original work. The design parameters based on the original work are given in Table 1. The values of the blade chord and twist distribution were calculated using the Horizontal Axis Rotor Performance Optimization (HARP\_Opt) code according to the designed parameters. The HARP\_Opt is a BEMT and optimization algorithm based model for prediction of rotor performance metrics. Fixed pitch and fixed speed configuration were used for turbine designing. The blade angle and twist distribution results are given in Table 2. The 3D geometric model of the turbine is shown in Fig. 2. Two flow domains were developed around the TCT to have one rotating

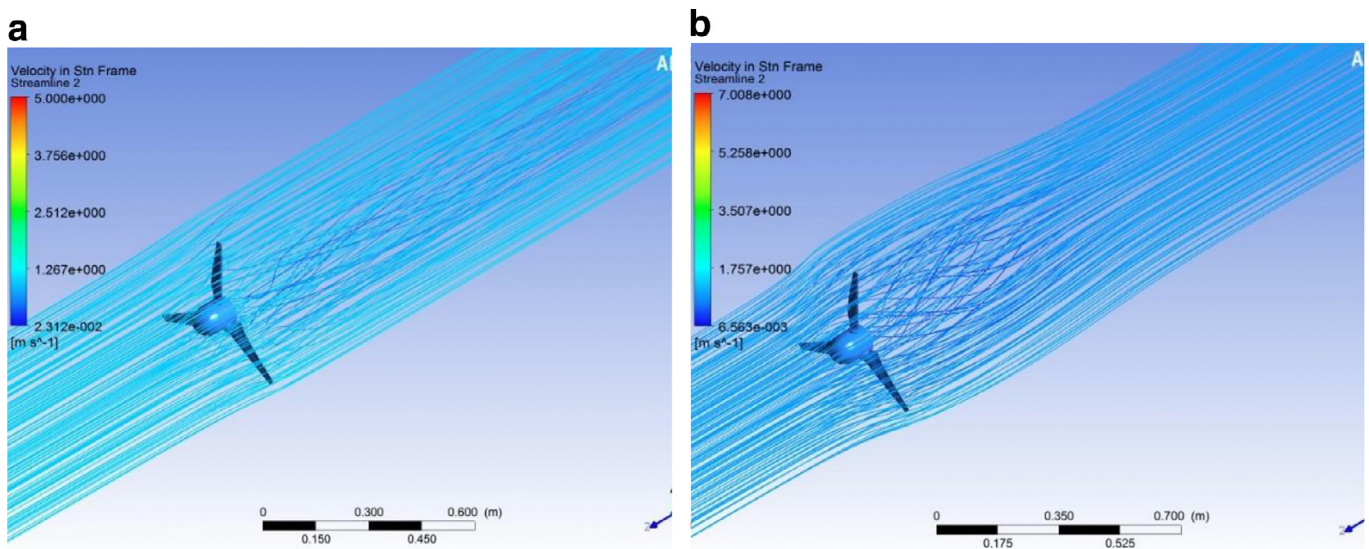


Fig. 6. Streamlines distribution around TCT system (a) at  $\lambda=2$  (b) at  $\lambda=5$ .

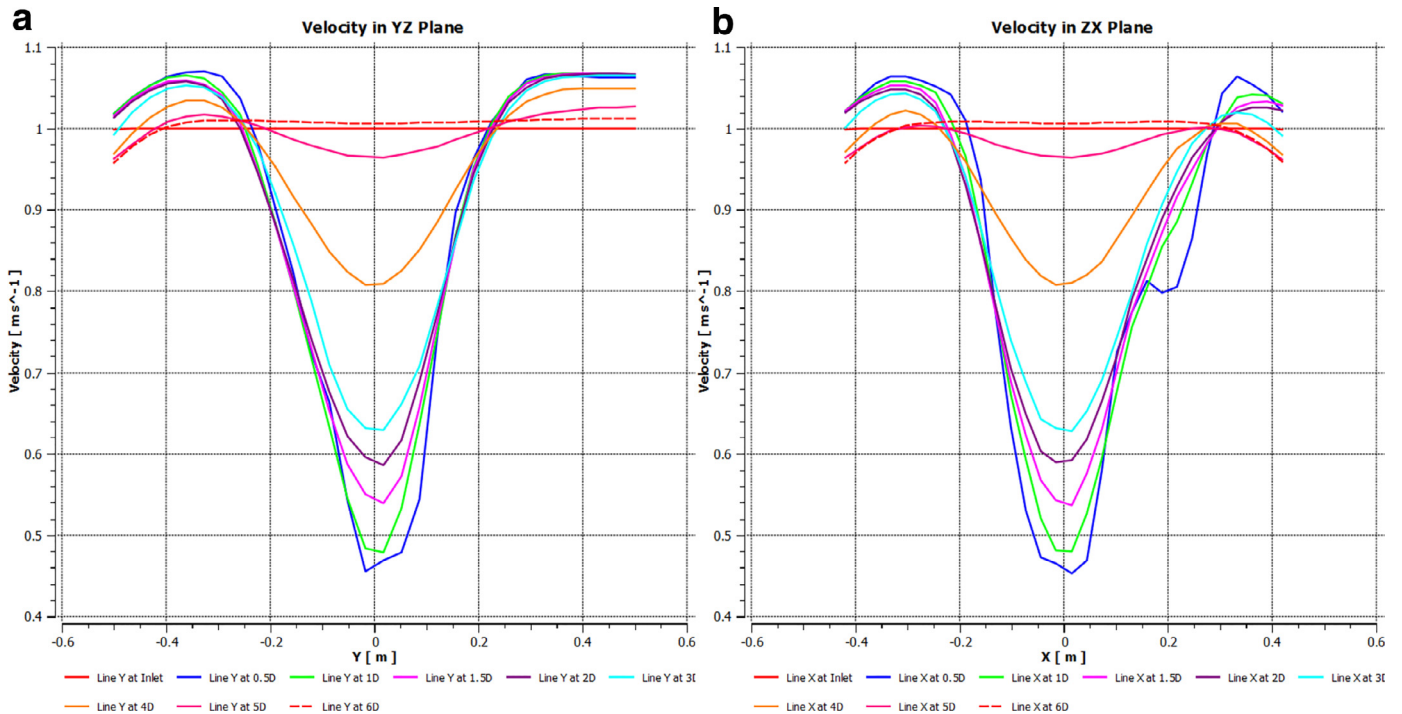


Fig. 7. Flow Velocity at  $\lambda=5$  (a) in YZ plane (b) in ZX plane.

and one stationary domain. The stationary fluid domain was modeled in a rectangular shape having the dimensions of 5 m length, 1 m width and 0.8 m height, whereas the rotating domain was modeled in a circular shape having the dimensions of 0.6 m diameter and 0.11 m height. Both domains are shown in Fig. 3.

2.2. Grid generation

A grid system was generated in ANSYS ICEM CFD, discretizing the turbine and fluid domain surfaces. A structured mesh was produced around the blade and hub, while on the fluid domains grids were unstructured. The overall numbers of tetrahedral elements were 4.7 million for whole TCT model. A dense prism-layer grid, consisting of 99,266 nodes and 197,474 elements was composed around the blades for torque prediction that occurs on blades. An unstructured tetra-prism grid, consisting of 1,312,011 nodes and 3,979,481 elements for rotating domain and 102,214 nodes and 541,280 elements for the stationary domain were composed. The mesh system for blade and fluid domain is shown in Fig. 4.

2.3. Boundary conditions

The CFD analysis was performed to investigate the flow behavior around the TCT. For this analysis in ANSYS CFX, uniform flow of 1 m/s with 5% turbulence intensity was specified normal to the inlet. Inflow velocity of 1 m/s is our designed velocity for TCT. No slip wall condition was set for hub and blade, while the fluid domain top free slip wall condition was defined. Opening pressure and zero gradients

Table 2  
Blade chord and twist distribution results.

Station	r/R	Radius (mm)	Chord (m)	Twist Angle (deg)
1	0.22	0.055	0.055364	16.95306
2	0.26	0.065	0.053791	15.57584
3	0.3	0.075	0.052075	14.27066
4	0.34	0.085	0.050243	13.04085
5	0.38	0.095	0.048318	11.88887
6	0.42	0.105	0.046322	10.8164
7	0.46	0.115	0.044273	9.824262
8	0.5	0.125	0.042188	8.912484
9	0.54	0.135	0.040077	8.080252
10	0.58	0.145	0.037953	7.325935
11	0.62	0.155	0.035822	6.647077
12	0.66	0.165	0.033689	6.040399
13	0.7	0.175	0.031556	5.501798
14	0.74	0.185	0.029421	5.026349
15	0.78	0.195	0.027282	4.608302
16	0.82	0.205	0.025131	4.241085
17	0.86	0.215	0.02296	3.917302
18	0.9	0.225	0.020756	3.628732
19	0.94	0.235	0.018505	3.366334
20	0.98	0.245	0.016189	3.120241

were selected in pressure and turbulence option respectively. A moving reference frame (MRF) was specified to simulate the turbine rotation in steady state condition. The alternate rotation model was applied to the inner rotating domain. 101.325 kPa reference pressure was selected in the pressure of the domain model and non-buoyant was selected in Buoyancy model option. Shear Stress Transport (SST) and automatic wall function were used for turbulence model. The choice of turbulence models for a flow analysis depends on the physics

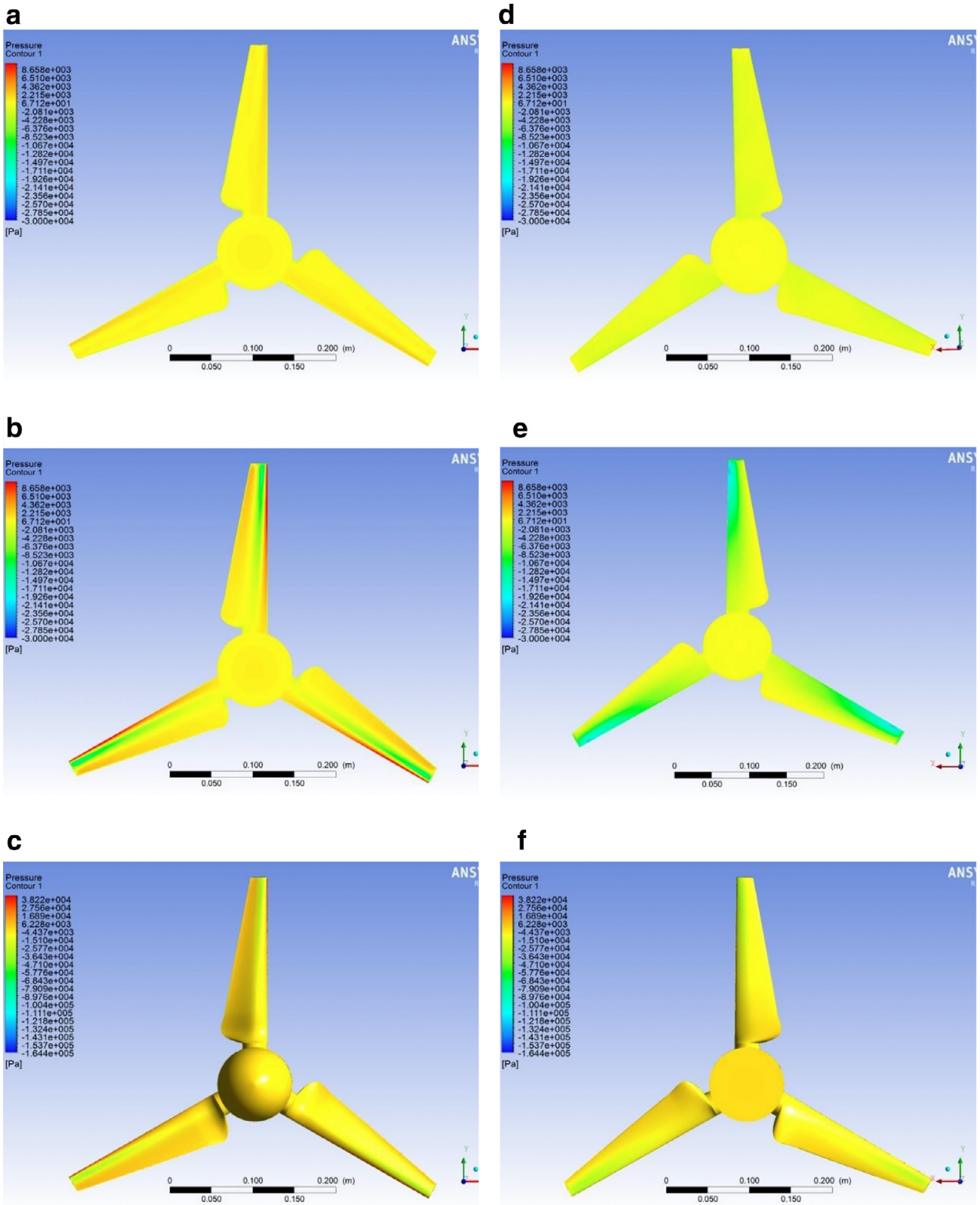


Fig. 8. Pressure on acting side and suction side (a) pressure side at  $\lambda=2$  (b) pressure side at  $\lambda=5$  (c) Pressure side at  $\lambda=9$  (d) suction side at  $\lambda=2$  (e) suction side at  $\lambda=5$  (f) suction side at  $\lambda=9$ .

Table 3  
Mechanical and fatigue properties of stainless steel [36].

Mechanical properties		Fatigue properties	
Parameter	Value	Alternating stress (MPa)	Number of cycles
Density	7750 kg/m <sup>3</sup>	202.5	93,600
Poisson Ratio	0.3	162	150,535
Modulus of Elasticity	205.6 GPa	121.5	607,940
Yield Strength	697.3 MPa	114.69	731,590
Ultimate Tensile Strength	891 MPa	97.865	1,206,290
		94.48	2,483,395
		87.72	3,200,090

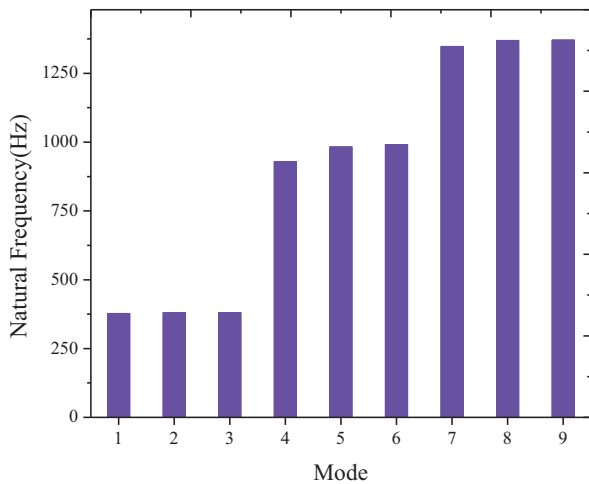


Fig. 9. Modal frequencies for different mode shapes.

of the problem, level of accuracy and available computational resources. The SST model is preferred for the flows involving flow separation and adverse pressure gradients. At boundary layer the  $k - \omega$  model has better accuracy than  $k - \epsilon$ , hence it has better accuracy for flow with moderate adverse pressure gradient but fails for flows with pressure induced separation. In addition, the  $k - \omega$  equation shows a strong sensitivity to the values of  $\omega$  in the free stream outside the boundary layer. The SST model overcome all these deficiencies and accurately predict the turbulence near the wall region and also far fields areas [34–38] This difference makes the SST model more suitable for a variety of flows than other models. And according to many researcher SST model is widely used in industry to accurately predict the turbulence near the wall region and far field areas.

In order to setup the flow analysis the outer domain was set stationary for the incoming flow field, while the inner domain was set to rotate for maximum power production.

In ANSYS-CFX solver control setting, the minimum iteration was defined 1, while the maximum iteration was defined 300 with the auto time scale. The residual, convergence criteria were set to  $10^{-4}$ . RMS as a residual type in convergence criteria and in equation class setting, the high-resolution option was used in the advection scheme. Rotor torque was added to output control to view the rotor torque after all iterations like other residuals.

The modal analysis was performed on the TCT to examine the mode shapes and natural frequencies. Since in most case, fewer initial mode shapes are important, therefore 9 modes were extracted in the analysis. In order to achieve the supporting condition of the turbine in operation, the back side of the hub was fixed. The rotational velocity of 20 rad/s was specified because at this rotational speed the turbine gives maximum power.

For fatigue analysis, the load was imported into Static Structural from the solution of CFX in the form of pressure. The imported load was applied on the surfaces of blades and the hub for inflow velocity of 1 m/s. The maximum coefficient of performance was observed at 20 rad/s. So, for fatigue analyses, the rotational velocity of 20 rad/s was specified. Fixed support was defined at the back surface of the hub. The solution was then run, and results were obtained in the form of stress intensity. The fatigue tool was used to predict the fatigue life of the turbine. In fatigue tool, the load ratio 0.1 is used due to the fluctuation of the hydrodynamic load. The value of alternating stress was varied by changing the scale factor in the fatigue analysis. A scale factor is a number by which alternating stress is multiplied to increase or decrease the load value for fatigue analysis. Then, fatigue life based on stress is predicted. The mechanical and fatigue properties of the selected material are given in Table 3.

### 3. Hydrodynamic analysis

#### 3.1. Performance of TCT

The performance of TCT is predicted through BEMT and CFD methods at 1 m/s inflow velocity. For CFD method, the torque values at different tip speed ratios ( $\lambda$ ) are calculated from the function calculator of ANSYS CFX. The following equations were used to calculate  $\lambda$  and  $c_p$  values

$$\lambda = \frac{\omega r}{v}; \quad c_p = \frac{2\tau\omega}{\rho A v^3}$$

Where  $\omega$  is the rotational speed of the turbine,  $r$  is the radius of the turbine,  $v$  is inflow velocity,  $\tau$  is torque,  $A$  is turbine area, and  $\rho$  is the density of water.

The performance curve for both cases is shown in Fig. 5. The good agreement between CFD and BEMT models validate the results. The  $c_p$  value for TCT increases with  $\lambda$  but after reaching the maximum value of 0.43 at  $\lambda=5$  then it

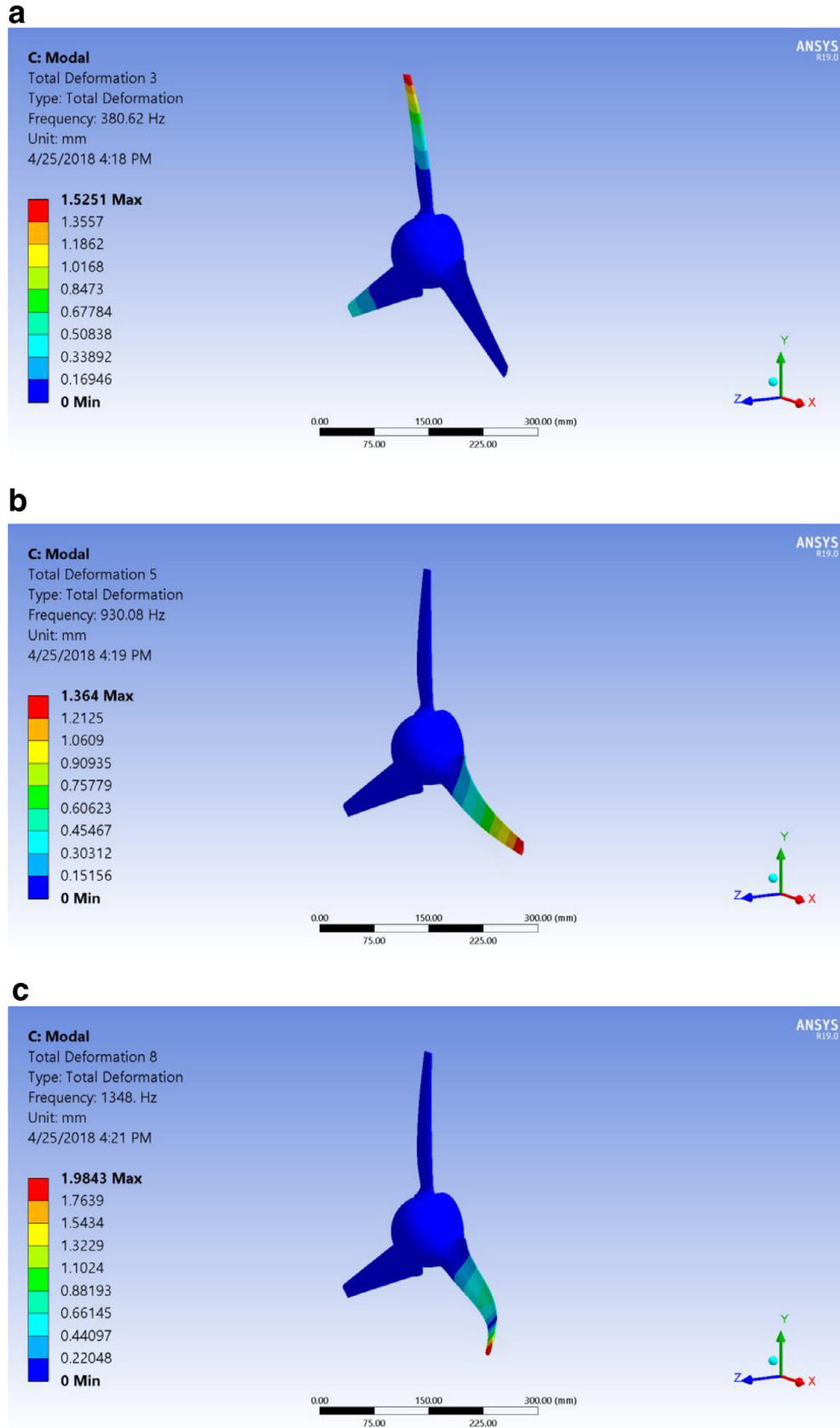


Fig. 10. Natural frequency response (a) Mode 1, (b) Mode 4 and (c) Mode 7.

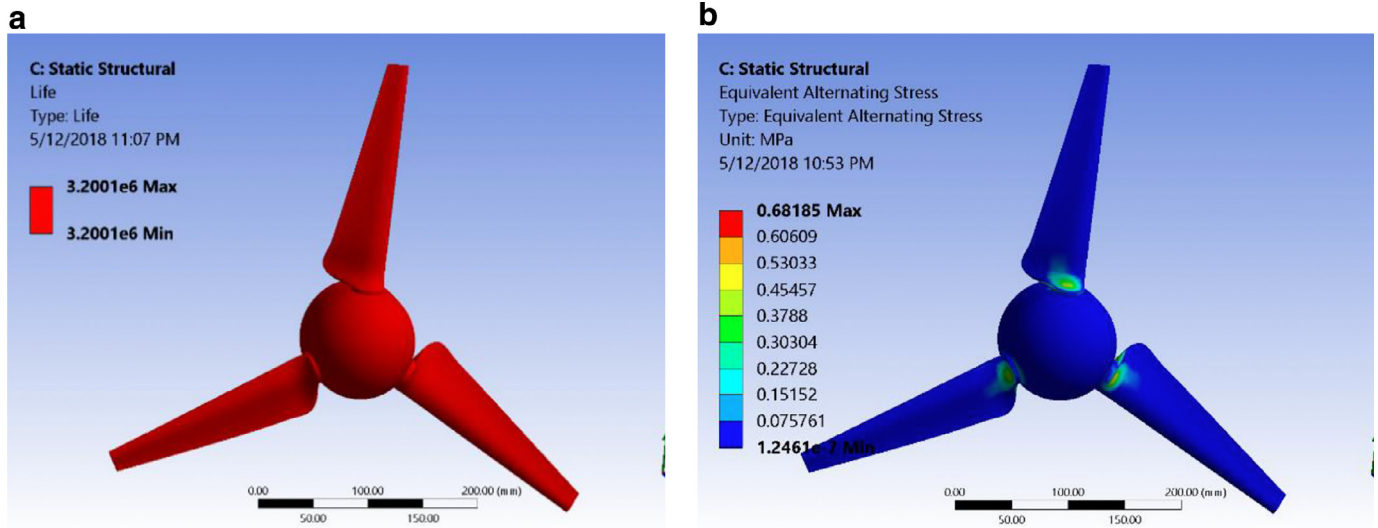


Fig. 11. Fatigue test results at operating loading condition (a) life (b) alternating stress.

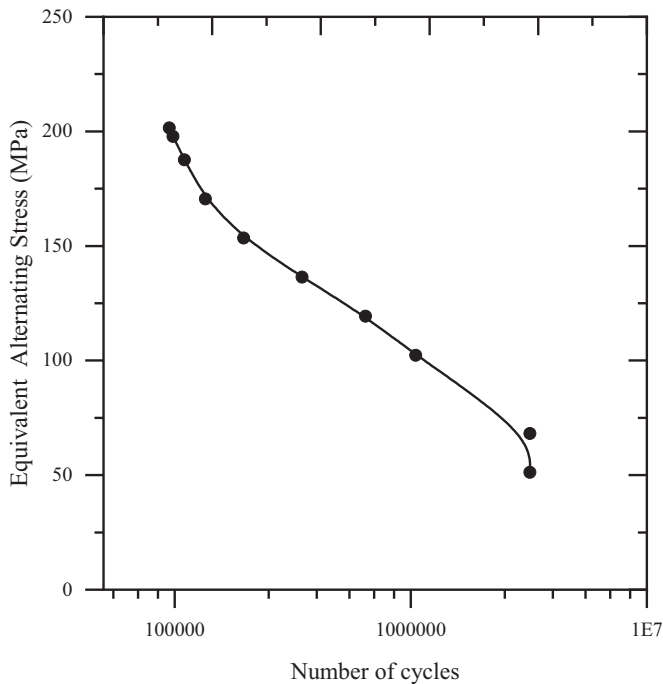


Fig. 12. Stress life prediction of TCT.

starts decreasing. The maximum value of  $c_p$  is achieved at  $\lambda=5$  which is Betz’s limit. At higher values of  $\lambda$  i.e., 6, 7, and 8 the  $c_p$  value keeps decreasing as shown in Fig. 5.

### 3.2. Streamlines distributions and velocity deficit around TCT

The swirling effect increases with an increase in  $\lambda$  as shown in Fig. 6. From the figure, it is disillusioned that the swirling effect is maximum at the near wake of the turbine, but at the far wake, the flow tends to recover its original shape and hence the swirling effect is reducing.

The inflow velocity decreases when water passes through the walls of the turbine. The decrease in inflow velocity (velocity deficit) after the turbine is converted into hydrokinetic energy of the turbine. The velocity deficit is observed due to the conversion of hydrokinetic energy to useful work. The variation of flow velocities between inlet and outlet is shown in Fig. 7.

### 3.3. Pressure distributions on TCT rotor

The lift force is produced due to the pressure difference of fluid corresponding to the asymmetric cross-sectional area and shape of the airfoil. The positive pressure at the leading edge and negative pressure at the trailing edge of the blade increase with an increase in the value of  $\lambda$ . The pressure difference between the suction side and pressure side reduces above  $\lambda=5$ . Hence the maximum performance is achieved at  $\lambda=5$ . The pressure at the pressure side and suction side are shown in Fig. 8.

## 4. Modal analysis

Three sets of modal frequencies with a slight variation are visualized due to the symmetry in the turbine model. Three frequencies in each set are due to presences of three blades in the turbine. Natural frequency response is shown in Fig. 9.

The mode shape 1, 4 and 7 are shown in Fig. 10(a), (b) and (c), respectively. In the first three modes, the blades of the turbine vibrate in the  $z$ -direction. In next three modes, i.e., mode 4, 5 and 6, the blades vibrate in the plane of rotation and finally, in mode 7, 8 and 9 the blade vibrates in the  $z$ -direction in a sinusoidal wave-like pattern. At 20rpm speed of the turbine which the operating speed of the turbine of the maximum coefficient of performance. The frequency of the applied load due to the flow of fluid will be around 0.33 Hz, as the applied load’s frequency is well below the

natural frequencies of the turbine so, the turbine will not resonate and therefore, it is safe.

## 5. Fatigue analysis

At operating loading conditions no failure occurs and the infinite life is achieved. For fatigue analysis, load in  $z$ -direction was considered. The stress-life fatigue model was used for simulation. At actual load, due to the pressure distributions, the life and alternating stress are given in Fig. 11. The life of TCT remains infinite from 0.68185 MPa to 68.185 MPa. However, the factor of safety decreases from 15 to 1.2865 which further reduces at higher loading conditions. The reduction in the factor of safety due to an increase in the stress value as scale factor was increased to observe the effect of load. The maximum stress concentration due to the fatigue loading is at blade root of TCT, which means that the blade failure will occur at blade root if the load is further increased. This location of stress concentration makes sense because the blade is under bending deflection due to action the FSI load. The  $S$ - $N$  curve based on stress life model is shown in Fig. 12.

## 6. Conclusion

A three-bladed HATCT was designed using the HARP\_Opt code. The CFD analyses were performed to investigate the performance, velocity and pressure distributions around the TCT. It was found that the swirling effect increases with an increase in  $\lambda$ . Positive pressure at the leading edge and negative pressure at the trailing edge increased by increasing the value of  $\lambda$ . However, the pressure difference between the suction side and pressure side reduces after passing through  $\lambda=5$ . Hence maximum efficiency was achieved at  $\lambda=5$ . Therefore, modal and fatigue behaviors were investigated at  $\lambda=5$ .

The mode shapes and the natural frequencies resulting from the modal analysis show that under the applied loading and operating conditions, the turbine's natural frequency is far from the external frequencies that will result from the turbine rotation, therefore, the turbine will not experience resonance and it will be safe to operate under the mode of vibration.

The results of fatigue analyses predict that the TCT remains in endurance limit at the higher load than operating loading conditions, therefore, the blades of the turbine should be hollow to save the material and reduce the weight of TCT. The stress concentration at blade root depicts that the blade root must be kept stronger to ensure TCT safety.

## References

- [1] M. Kamran, M. Mudassar, S.R. Ahmed, H.S. Mehmood, F.M. Joyia, M. Hussain, H. Ahmad, S. Saeed, *Int. J. Renew. Energy Res.* 9 (2019) 301–308.
- [2] M.M. Ahsan, M. Zulqernain, H. Ahmad, B.A. Wajid, S. Shahzad, M. Hussain, *Int. J. Renew. Energy Res.* 9 (2019) 343–353.
- [3] F.O. Rourke, F. Boyle, A. Reynolds, *Appl. Energy* 87 (2010) 398–409.
- [4] P. Ouro, M. Harrold, T. Stoesser, P. Bromley, *J. Fluids Struct.* 71 (2017) 78–95.
- [5] S. Zanforlin, *Ocean Eng.* 156 (2018) 358–372.
- [6] P. Ouro, M. Harrold, T. Stoesser, P. Bromley, *J. Fluids Struct.* 71 (2017) 78–95.
- [7] J. Liu, H. Lin, S.R. Purimitla, E.T. Mohan Dass, *Appl. Ocean Res.* 64 (2017) 58–69.
- [8] L. Chernin, D.V. Val, *Renew. Energy* 113 (2017) 688–696.
- [9] R.F. Nicholls-Lee, S.R. Turnock, S.W. Boyd, *Renew. Energy* 50 (2013) 541–550.
- [10] J.N. Goundar, M.R. Ahmed, *Appl. Energy* 111 (2013) 161–174.
- [11] E.M. Fagan, C.R. Kennedy, S.B. Leen, J. Goggins, *Renew. Energy* 97 (2016) 358–372.
- [12] C.R. Kennedy, V. Jaksic, S.B. Leen, C.M.Ó. Brádaigh, *Renew. Energy* 121 (2018) 688–699.
- [13] T. Blackmore, L.E. Myers, A.S. Bahaj, *Int. J. Mar. Energy* 14 (2016) 1–26.
- [14] G. McCann, M. Thomson, S. Hitchcock, G. Hassan, in: *Proceeding of the Second International Conference on Ocean Energy*, 2008, pp. 15–17.
- [15] M. Hussain, R. Khan, N. Abbas, *J. King Saud Univ. – Sci.* 31 (2019) 222–229.
- [16] B.S. Kim, S.Y. Bae, W.J. Kim, S.L. Lee, M.K. Kim, in: *Proceeding of the IOP Conference Series on Earth and Environmental Science*, 15, 2012.
- [17] K.-P. Kim, M.R. Ahmed, Y.-H. Lee, *Renew. Energy* 48 (2012) 557–564.
- [18] R. Malki, A.J. Williams, T.N. Croft, M. Togneri, I. Masters, *Appl. Math. Model.* 37 (2013) 3006–3020.
- [19] I. Masters, A. Williams, T. Croft, M. Togneri, M. Edmunds, E. Zangiabadi, I. Fairley, H. Karunarathna, *Energies* 8 (2015) 7833–7853.
- [20] E.P.N. Duque, M.D. Burklund, W. Johnson, in: *Proceeding of the ASME 2003 Wind Energy Symposium*, ASME, 2003, pp. 43–61.
- [21] Q. Hu, Y. Li, Y. Di, J. Chen, *J. Renew. Sustain. Energy* 9 (2017) 064501.
- [22] R.F. Nicholls-Lee, S.R. Turnock, S.W. Boyd, in: *Proceeding of the Ninth European Wave Tidal Energy Conference*, 2011, pp. 1–8.
- [23] F. Jing, W. Ma, L. Zhang, S. Wang, X. Wang, *J. Hydrodyn. Ser. B* 29 (2017) 109–117.
- [24] C.H. Jo, J.Y. Yim, K.H. Lee, Y.H. Rho, *Renew. Energy* 42 (2012) 195–206.
- [25] J. Liu, H. Lin, S.R. Purimitla, M.D. E.T., *Appl. Ocean Res.* 64 (2017) 58–69.
- [26] A. Olczak, T. Stallard, T. Feng, P.K. Stansby, *J. Fluids Struct.* 64 (2016) 87–106.
- [27] M. Edmunds, R. Malki, A.J. Williams, I. Masters, T.N. Croft, *Int. J. Mar. Energy* 7 (2014) 20–42.
- [28] P. Liu, N. Bose, in: *Proceeding of the Third International Symposium on Marine Propulsors*, 2013, pp. 242–256.
- [29] C.-H. Jo, J.-H. Lee, Y.-H. Rho, K.-H. Lee, *Renew. Energy* 65 (2014) 175–182.
- [30] T.O. 'doherty, A. Mason-Jones, D.M. O 'doherty, C.B. Byrne, I. Owen, Y.X. Wang, in: *Proceeding of the Eighth European Wave Tidal Energy Conference (EWTEC)*, 2009, pp. 1–9.
- [31] C.-H. Jo, D.-Y. Kim, Y.-H. Rho, K.-H. Lee, C. Johnstone, *Renew. Energy* 54 (2013) 248–252.
- [32] C. Jo, K. Lee, S. Hwang, D. Kim, in: *Proceeding of the 2015 IEEE Fifteenth International Conference on Environmental and Electrical Engineering, IEEE*, 2015, pp. 472–477.
- [33] B. Kim, W. Kim, M. Kim, in: *Proceeding of the Third International Conference on Ocean Energy*, 2010, pp. 3–6.
- [34] M. Badshah, J. VanZwieten, S. Badshah, S. Jan, *IET Renew. Power Gen.* (2019).
- [35] F.R. Menter, M. Kuntz, R. Langtry, *Turb. Heat Mass Transf.* 4 (2003) 625–632.
- [36] S. Gorji, M. Seddighi, C. Ariyaratne, A.E. Vardy, T.O. Donoghue, D. Pokrajac, S. He, *Comput. Fluids* 89 (2014) 111–123.
- [37] T. Aized, K. Hassaan, *Arab. J. Sci. Eng.* (2019).
- [38] N. Radu, M. Liviu, M. Sebastian, N. Pasca, *Renew. Energy* 9 (2013) 413–420.